Numerical investigation of the effects of orientation and gravity in a Closed Loop Pulsating Heat Pipe

Mauro Mameli, Marco Marengo, Stefano Zinna

Department of Industrial Engineering, University of Bergamo. Viale Marconi 5, 24044 Dalmine (BG), Italy.

mauro.mameli@unibg.it, marco.marengo@unibg.it, stefano.zinna@uniheat.it

ABSTRACT

The Closed Loop Pulsating Heat Pipe (CLPHP) is a very promising passive two-phase heat transfer device for relatively high heat fluxes (up to 30W/cm^2) first patented by Akachi (1990). Although the CLPHP has a simple structure, its working principles are very complex compared to the standard heat pipe with a porous wick. One of the most debated issues deals on how the thermal performance is affected by the inclination and by the action of different gravity fields (terrestrial, lunar, martian and microgravity). Even if the internal tube diameter satisfies the conventional slug flow regime requirement on the Bond number, gravity force still plays an important role on the PHP behaviour. Heat input and the number of turns are two of the most important indirect parameters linked to the gravity issue. A complete numerical campaign has been performed by mean of a FORTRAN code for different inclination and gravity level on various PHP. The numerical model is able to estimate both the hydrodynamic and the thermal performance of a CLPHP with different working fluids. The analysis of the results shows the effect of local pressure losses due to bends is important and must be taken into account, in particular in the horizontal operation which is the reference point for space applications. Numerical results are matched with the experimental data quoted in literature and both good qualitative and quantitative agreement have been found.

Keywords: *passive device, slug flow, numerical simulation.*

Nomenclature

A, Area [m^2];
c_p, Specific heat [J/kgK];
d, Diameter [m];
f, Friction factor [-];
g, Gravity acceleration [m/ s^2];
h, Heat transfer coefficient [W/m^{2}K];
H, Enthalpy, [J/kg.K]
k, Thermal conductivity [W/mK];
L, Length [m];
m, Mass [kg];
$\dot{m}$, Mass flow rate [kg/s];
n, Number of computational grids [-];
P, Pressure [Pa];
p, Tube perimeter [m];
Pr, Prandtl number [-];
q", Heat flux [W/ cm^2];

$\dot{Q}$,Heat input [W];
R, Ideal gas constant for water [J/kg.K];
Re, Reynolds number [-];
r_{fs}, Surface roughness [m];
T, Temperature [°C];
$\overline{T}$, Mean Steady State Temperature [°C];
V, Volume [m^3];
x, Vapor mass quality [kg_{vap}/kg_{tot}];
z, Axial direction coordinate [m];
δ, Thickness [m];
γ, Filling ratio [-];
μ, Dynamic viscosity [Pa.s];
ρ, Density [kg/m^3];
σ, Surface tension [N/m];
τ, Shear stress [N/m^2];

Subscripts

b, back meniscus;
co, condenser/condensation;
cr, channel cross section;
crit, critical;
eq, equivalent;
ev, evaporator/ evaporation;
exp, experimental;
f, front meniscus;
fluid, related to fluid;
film, liquid film;
g, gravitational;
i, liquid slug index;
∞, Ambient;
j ,vapor plug index;
k, turn-bend grid index
l, liquid;
lv, liquid-vapor;
min, Minimum;
max, Maximum;
num, numerical;
rad, radial;
sat, Saturation;
s, liquid slug grid;
t, turn;
tot, total;
v, vapor;
vp, vapour plug;
w, tube wall;
0, initial;

INTRODUCTION

The Pulsating Heat Pipe (PHP) usually consists of a small diameter meandering copper tube which can be in the form of closed loop (CLPHP) or in the form of an

open loop with closed ends (OLPHP), evacuated and then partially filled with a working fluid. If the internal diameter is less than the critical value obtained from equation (1):

$$d_{crit} \approx 2\sqrt{\frac{\sigma}{g(\rho_l - \rho_v)}} \quad (1)$$

the fluid resides inside the tube as an alternation of liquid slugs and vapour plugs. Then, when the device gets in contact with a heat source, the fluid starts to oscillate and circulate chaotically within the tube allowing the heat transfer to the colder zone. Experimental works in literature show that the PHP could be suitable for a wide range of industrial heat transfer applications.

- Electronic cooling:

Miyazaki (2005) developed a series of flexible CLPHP for notebook PC cooling that can dissipate heat from the CPUs to the rear surface of the foldable display. Woo et al. (2008) showed that a PHP can be embedded inside heat sinks in order to improve their cooling performance.

- Solar heat recovery:

Rittidech et al. (2007) investigated a flat plate solar collector in conjunction with a OLPHP operating with R134a as a working fluid and showed that this solution offers a reasonably efficient and cost effective alternative with respect to solar collector systems equipped with standard heat pipes.

- Heat exchangers:

Khandekar (2010) presented a temperature controlled liquid-liquid PHP module which can be suitable for process waste heat recovery and a heat flux controlled air cooled PHP module that can dissipate up to 800W.

Actually few experimental data are available to understand the PHP behaviour at zero gravity level. Gu et al. (2004, 2005) tested a PHP in microgravity conditions by mean of parabolic flight campaigns but the zero-g period of a parable (22 seconds) do not seem to be enough to cover the PHP transient period.

Many attempts of theoretical modeling have been carried out in the last two decades: Zuo et al. (2001) developed a one dimensional model for the thermal-hydraulic simulation of PHPs but only the thermal performance over filling ratio has been experimentally validated; Shafi et al. (2001) presented a multi-plug model with heat transfer both for the OLPHP and the CLPHP. Although the authors consider many characteristic parameters, results show that the total

number of vapor plugs always reduces to the total number of heating sections after a few seconds of simulation time; Zhang and Faghri (2003) proposed a multi-plug model of CEPHP and investigated the effect of the number of turns on the fluid oscillation frequency; Holley and Faghri (2005) developed one of the most comprehensive models of CLPHP working with water but only a qualitative validation is provided; Sakulchangsatjatai et al. (2008) developed an OLPHP model based on Shafii et al. (2001) and on Zhang and Faghri (2003) by adding empirical assumptions on nucleate boiling frequency, bubble length and film thickness coming from an experimental visualization. Qualitative and quantitative validation was given for evaporator temperatures, inclination angles and input heat fluxes; Khandekar and Groll (2008) suggested a fully lumped parameters model for the single closed loop PHP but their hypothesis of homogeneous fog-flow seems more suitable for thermosyphons.

In the present work the numerical code of Holley and Faghri (2005) and its latest improved version (Mameli et al. 2010) are tested on different parameters which are directly or indirectly involved by the gravity level. The twofold aim is to show that the PHP technology could be a good candidate for space applications and how much could be the decrement of performances due to different gravity values and inclinations.

MATHEMATICAL AND NUMERICAL MODEL

Holley and Faghri (2005) developed a one dimensional separated flow model of a close loop PHP working with water which represents the starting point of the present analysis. The main novelties with respect to the past are: i) the possibility of choosing between different working fluids, ii) a non-homogeneous heat transfer sub-model with updated heat transfer correlations, iii) the presence of pressure drops on the liquid phase due to meanderings. This section is devoted to describe the improved theoretical and numerical model in the form used for the simulations.

The fluid is represented by an alternation of liquid slugs (index *i*) and vapor plugs (index *j*) which are always traceable during the simulations. Figure 1 shows the back and forward menisci locations for the i-th liquid slug and the main heat transfer paths.

The tube wall is subdivided into control volumes which are fixed in space (eulerian approach), while the fluid control volumes follow the liquid slugs and

vapor plugs which can move, expand, nucleate and collapse (lagrangian approach). This allows the user to know exactly where the liquid slugs and vapor plugs are located along the tube at each simulation time step.

Since the tube is closed in a loop, the “entrance” 0 and the “exit” L are set as the same reference point which is the origin. After solving the momentum equation for each liquid slug, the updated position of the menisci may be smaller than zero or bigger than L. This means relatively that a liquid slug is coming back through the origin or it is trespassing it. For this reason a dedicated wrap function redefines the menisci locations at each time step as follows:

$z_{new} = z$ when $0 < z < L$;

$z_{new} = z + L$ when $z < 0$;

$z_{new} = z - L$ when $z > L$;

$z_{new} = 0$ when $z = L$.

Where z refers to the position of the forward or backward meniscus related to the i-th liquid slug.

The tube has constant cross sectional area and no porosity of the wall is considered (i.e, there is no porous wick and therefore its working principles are really different from a sintered or mesh heat pipe).

The main assumptions are listed below:

a) Derivatives of density and viscosity are assumed negligible. However, all the fluid thermo-physical properties are evaluated as functions of temperature.
b) The momentum equation for the liquid slug is lumped (advection term is neglected)
c) The model is 1-D, with the axial dimension (z) along the flow path considered for momentum and heat transfer; heat transfer in the radial direction is lumped.
d) The forward and backward menisci of the liquid slugs are assumed to maintain a spherical meniscus shape with zero contact angle at the wall.
e) Surface tension is evaluated at the vapor plug temperature.
f) The pressure within each vapor plug is assumed uniform.
g) Vapor exists at saturated conditions; each vapor plug is treated as an ideal gas and has negligible flow friction with the wall.
h) The liquid film which surrounds each vapor plug is only considered for the heat transfer purpose, but does not play any role in the hydrodynamics and in

terms of liquid mass and momentum.

The governing equations are listed here below:

Momentum equation for the i-th liquid slug

The momentum equation for incompressible flow in a circular pipe is:

$$\rho \frac{Du_l}{Dt} = \rho g \cos\theta - \frac{dP}{dz} + \frac{\tau}{d} \tag{2}$$

where $\frac{Du_l}{Dt} = \frac{\partial u_l}{\partial t} + u_l \frac{\partial u_l}{\partial z}$ is the total derivative. By mean of assumptions a) and b) and writing the slug velocity as:

$$u_l = \dot{m}_l / \rho A_{cr} \tag{3}$$

the momentum equation turns into the following ordinary differential equation which is applied to each i-th liquid slug:

$$\left[\frac{d\dot{m}_l}{dt} = A_{cr} (\Delta P_g - \Delta P_v + \Delta P_\tau + \Delta P_K) \right]_i \tag{4}$$

Note that the liquid slug is treated with a lumped parameter approach. The liquid slug will be subdivided into a number n_s of smaller control volume only for solving the energy equation (see energy equation for the liquid slug).

The different pressure terms on the right hand side are respectively due to:

Gravity force

$$\Delta P_g = \rho_l g L \cos\theta \tag{5}$$

Where *θ[deg]* is the angle between the gravity vector and the flow direction.

Adjacent vapour plugs expansion/compression

$$\Delta P_v = \left[P_{sat}(T_v) \right]_{j+1} - \left[P_{sat}(T_v) \right]_j \tag{6}$$

Viscous shear

$$\Delta P_\tau = \frac{f}{2d} \rho_l u_l^{\,2} \tag{7}$$

Where the friction factor f is evaluated for the laminar and turbulent regimes as follows:

$$f = 64/\mathrm{Re}_l \quad \text{when} \quad \mathrm{Re}_l < 2000 \tag{8a}$$

$$\frac{1}{\sqrt{f}} = 1.74 - 2\log_{10}\left(\frac{2k_s}{d} + \frac{18.6}{\mathrm{Re}_l\sqrt{f}}\right) \quad \text{when} \quad \mathrm{Re}_l \geq 2000 \tag{8b}$$

Minor losses due to bends and turns

When the number of turns increases, the pressure losses related to the bends and turns in a PHP are not negligible and must be taken into consideration. k is the index related to the turns.

$$\Delta P_K = \sum_{k=1}^{N_t} \frac{K_k}{2d} \rho_l u_l^{\,2} \tag{9}$$

This term is non-zero only if the i-th liquid slug is passing in between the turn boundaries $[Z_{K,b};\ Z_{K,f}]_k$ (fig.2); note that a single Liquid Slug can pass through more than one turn and thus it can undergo more than one pressure drop.

The constant K_k is the loss coefficient due to the k-th turn according to Darby (1999,2001):

$$K_k = \frac{K_{\mathrm{Re}}}{\mathrm{Re}_l} + K_r\left(1 + \frac{K_d}{(d/0.0254)^{0.3}}\right) \tag{10}$$

This empirical correlation depends on three main parameters (K_{Re} , K_r , K_d), on the Reynolds number and on the exact geometry of the bend. The values adopted for the three parameters in case of 90° bend and 180° are listed in table 1.

The 3-K method considers that the flow regime may be variable: K_k is indeed unaffected by Reynolds number when $Re >> K_{Re}$ (turbulent flow), however K_k grows as soon as $Re < K_{Re}$. This must be taken into account since the local Reynolds number related to each slug is often laminar. The K_r constant is linked to the fitting curvature ratio r_t/d and the fitting type: as the curve radius decreases, the sensitivity to surface roughness increases, thus K_k is greater for smaller bends of a given type. Furthermore the $d/0.0254$ correction accounts for the size differences: K_k is higher for small diameters and nearly constant for large sizes. The bends and turns lengths are discretized in the code: if one liquid slug is partially occupying one bend, than it consequently undergoes a lower pressure

drop. Due to assumption (d) and the constant cross section along the tube length, the pressure drop due to capillary forces is neglected. Further work is mandatory to investigate the pressure term due to advancing and receding angles of Taylor bubbles and implement them in the code.

Liquid slug merge

Also the merging of liquid slugs is accounted for. If the spacing between any two adjacent menisci is zero, or if there is overlap, the two liquid slugs are combined and the number of liquid slugs is reduced by one. The mass flow rate for the combined slug is determined by summing the momenta.

Vapor plug formation

Finally the formation of new vapor plugs has been taken into account only in terms of homogeneous nucleation inside the liquid phase. The exact interaction between the wall and fluid in the boiling process has still to be implemented. By the time being the new vapor plugs are located according to these steps:

- The temperature of each liquid sub-volume is compared to the temperatures of the vapor plugs adjacent to the liquid slug.
- The maximum grid boundary temperature is chosen as the location where a new plug is formed if that temperature exceeds one or the other adjacent plug temperatures. The mass flow rate is the same for both segments of the slug.
- The temperature of the plug is set to the fluid temperature at that location.

The other criterion for locating new vapor plugs is to compare the saturation pressure associated with the liquid slug grid boundary temperature to the pressure of the adjacent vapor bubble grid boundary.

$$\left[P_{sat}(T_l)\right]_{n_s} > \max\left[\left(P_{sat}(T_v)+\frac{2\sigma}{r}\right)_j;\left(P_{sat}(T_v)+\frac{2\sigma}{r}\right)_{j+1}\right] \tag{11}$$

If the above condition (11) occurs, a new vapor plug will be created and, if there is sufficient vapor pressure in the plug, the plug will grow, otherwise it will collapse and the two adjacent liquid slugs will merge again.

The displacements of the back menisci positions

The new positions of the liquid slug are calculated based on mass flow rate and time step by convergence of the following equation:

$$\Delta z_i = \frac{\Delta t}{2A_{cr}}\left(\frac{\dot{m}+\Delta\dot{m}}{\rho_l\left[T_l\left(z_{b,i}+\Delta z_i\right)\right]}+\frac{\dot{m}}{\rho_l\left[T_l\left(z_{b,i}\right)\right]}\right) \tag{12}$$

The initial estimate is:

$$\Delta z_i = \frac{\Delta t}{2A_{cr}}\left(\frac{\dot{m}+\Delta\dot{m}}{\rho_l\left[T_l\left(z_{b,i}\right)\right]}\right) \tag{13}$$

The back meniscus positions are updated:

$$z_{b,i} = z_{b,i} + \Delta z_i \tag{14}$$

The forward meniscus position is then calculated by mean of the conservation of mass at each time step.

Energy equation for the i-th liquid slug

The following partial differential equation accounts for heat storage and axial conduction within the fluid; the heat transfer between the wall and fluid $q_{w\text{-}f}$ is lumped (see the heat transfer between the tube wall and the working fluid paragraph).

$$\left[c_{p,l}\rho_l A_l \frac{\partial T_l}{\partial t} = q_{w-f}\, p + k_l A_l \frac{\partial^2 T_l}{\partial z^2}\right]_i \tag{15}$$

Each liquid slug is divided into n_s nodes and the temperature for each node is evaluated by integrating eq 15. The remaining spatial derivative is determined using a first order central difference. Values of heat transfer between the wall and fluid are interpolated based on the representative values of adjacent nodes.

Energy equation for the wall

Holley and Faghri (2005) assume that the internal tube surface is covered by a thin wick and that the liquid film surrounding each vapour bubble is always filling the porous structure. Since most of the prototypes and the experimental apparati are built with smooth tubes (this is also the most attractive feature of the CLPHP with respect to the standard heat pipe) the wick is not considered in the present work and the energy equation for the wall is:

$$c_{p,w}\rho_w A_w \frac{\partial T_w}{\partial t} = q_{ex}\, p_0 - q_{w-f}\, p + k_w A_w \frac{\partial^2 T_w}{\partial z^2} \tag{16}$$

where

$$q_{ex} = \begin{cases} q_{ev} & \text{evaporator zone} \\ 0 & \text{adiabatic zone} \\ h_{\infty}(T_{\infty} - T_w) & \text{condenser zone} \end{cases} \quad (17)$$

The entire wall tube is divided into n_w nodes and the temperature for node is evaluated by integrating equation (16). The remaining spatial derivative is determined using a first order central difference. Values of heat transfer between the wall and fluid are interpolated based on the representative values of adjacent grids.

Energy equation for the j-th vapour plug

The following partial differential equation accounts for heat storage within the entire vapour plug, for the heat transferred between vapor and the tube wall $q_{w\text{-}f}$ and for axial conduction with the neighbouring liquid slugs.

$$\left[(z_{f,j} - z_{b,j}) A_{cr} \frac{\partial}{\partial t} \left(H_v \frac{P_{sat}(T_v)}{R T_v} \right) = q_{w-f}\, p (z_{f,j} - z_{b,j}) + k_l A_l \left. \frac{\partial T_l}{\partial z} \right|_{Z_{f,i-1}} - k_l A_l \left. \frac{\partial T_l}{\partial z} \right|_{Z_{b,i}} \right]_j \quad (18)$$

Forward and backward first order differences are used for conduction at the menisci.

Heat transfer between the tube wall and the working fluid

When the local Reynolds number related to the i-th liquid slug is $Re_l < 2000$ and the liquid slug is heated or cooled by mean of sensible heat the local Nusselt number is far from being constant, thus the thermally developing laminar flow correlation by Shah (1975) has been implemented:

$$h_l = \begin{cases} \left(\frac{k_l}{d}\right) \cdot 1.953 \cdot \left(\mathrm{Re}_l \, \mathrm{Pr}_l \frac{D}{L_x} \right)^{1/3} \text{ when } \left(\mathrm{Re}_l \, \mathrm{Pr}_l \frac{D}{L_x} \right) \geq 33.3 \\ \left(\frac{k_l}{d}\right) \left(4.364 + 0.0722 \mathrm{Re}_l \, \mathrm{Pr}_l \frac{D}{L_x} \right) \text{when} \left(\mathrm{Re}_l \, \mathrm{Pr}_l \frac{D}{L_x} \right) \leq 33.3 \end{cases} \quad (19)$$

where L_x is the thermal entry length and it is set equal to the evaporator/condenser length.

For the transient/turbulent flow ($2000 \leq Re_l \leq 10000$) the Gnielinski correlation (Incropera et al. 2007) has been implemented:

$$h_l = \left(\frac{k_l}{d}\right)\left[\frac{(f/8)(\mathrm{Re}_l - 10^3)\mathrm{Pr}_l}{1+12.7(f/8)^{1/2}\left(\mathrm{Pr}_l^{2/3}-1\right)}\right] \tag{20}$$

For the fully turbulent flow ($Re_l \geq 10000$) the Dittus-Boelter correlation (Incropera et al. 2007) has been used:

$$h_l = \left(\frac{k_l}{d}\right)0.023\,\mathrm{Re}_l^{0.8}\,\mathrm{Pr}_l^{n} \tag{21}$$

where $n = 0.4$ if $T_w > T_{fluid}$ and $n = 0.3$ if $T_w < T_{fluid}$.

From the fluidmechanical point of view, the vapor plugs are made of vapor only, while from the heat transfer point of view, a thin liquid film is supposed to wet the inner tube surface sourrounding the vapor plugs and no slip exists between the phases (assumption h). Due to these assuptions each vapor plug is hence treated as a two-phase system in equilibrium where the local vapor mass quality x_{vp} is not calculated as the ratio of mass fluxes but simply as the ratio of masses; x_{vp} is then a function of the liquid film thickness δ_{film} and the fluid density which depends in its turn on the temperature. If δ_{film} is assumed constant along the vapour slug, then the local vapour mass quality can be estimated as follows:

$$x_{vp} = \frac{m_v}{m_t} = \frac{V_v \rho_v(T_{sat})}{V_v \rho_v(T_{sat}) + V_l \rho_l(T_{sat})} = \tag{22}$$

$$= \frac{\left(\frac{D}{2}-\delta_{film}\right)^2 \rho_v(T_{sat})}{\left[\left(\frac{D}{2}-\delta_{film}\right)^2 \rho_v(T_{sat})\right] + \left\{\left(\frac{D}{2}\right)^2 - \left[\left(\frac{D}{2}-\delta_{film}\right)^2\right]\rho_l(T_{sat})\right\}}$$

In figure 3 the vapor mass quality has been plotted as a function of the liquid film thickness for different fluid temperatures.

If the liquid film thickness could be easily mesured then the local vapor mass quality could be estimated by mean of equation 22 and fed into the semiempirical correlations for the two phase heat transfer (eq. 23 and 24). Even if δ_{film} is a crucial parameter and should not be a direct input for the code, it is also very difficult to measure experimentally. The last available measurements by Han and Shikazono (2009) for a 1.305 mm internal diameter tube working with air and ethanol in adiabatic conditions show that the valid range for δ_{film} is between 1 and

100 μm. This range has been taken as the reference for the simulations. In the present model the vapor mass quality of each vapor plug is assumed a priori on the basis of the following argument: if a vapor bubble is passing through the evaporator zone then the liquid film is subjected to relatively high temperatures and undergoes evaporation. Under these conditions (high temperature and thin liquid film due to the evaporation process), a high vapor mass quality x_{ev} can be chosen for the vapor plugs which are passing through the evaporator section. Viceversa in the condenser zone the lower average fluid temperature and the thicker liquid films lead to a very low vapor mass quality x_{co}.

Previous numerical investigations (Mameli et al. 2010) allowed to determine the average ranges of fluid temperature for each input heat flux $[T_{fluid,min}; T_{fluid,max}]$; the vapor mass quality ranges $[x_{vp,min}; x_{vp,max}]$ have been calculated with respect to these temperatures by using $\delta_{film,min} = 1\ \mu m$ and $\delta_{film,max} = 100\ \mu m$. The final vapor mass quality for the evaporating $x_{vp,ev}$ and condensing $x_{vp,co}$ vapor plugs have been chosen in between these ranges as shown in table 2.

Regarding the boilig/evaporation heat transfer, the Gungor and Winterton (Carey 2007) general correlation is used:

$$h_b = h_l \left\{ 1 + 3000 Bo^{0.86} + \left[\frac{x_{ev}}{1 - x_{ev}} \right]^{0.75} \left(\frac{\rho_l}{\rho_v} \right)^{0.41} \right\} \tag{23}$$

where $Bo = \frac{q'' A_{cross}}{|\dot{m}| H_{lv}}$ is the boiling number, x_{ev} is the vapor mass quality of the heated vapor plugs (taken from table 2) and h_l is the single phase (liquid) convection coefficient evaluated for the different flow regimes (eq. 19,20,21).

With regard to the condenser zone, the correlation for convective condensation by Shah(Carey 2007) has been implemented:

$$h_c = h_l \left[(1 - x_{co})^{0.8} + \frac{3.8 x_{co}^{0.76} (1 - x_{co})^{0.04}}{(P/P_{crit})} \right] \tag{24}$$

Where x_{co} (taken from table 2) is the vapor mass quality of the cooled vapor plugs. In light of such hypothesis the algorithm for the heat transfer subroutine is set as follows.

For the Liquid Slugs:

- If $T_w > T_{fluid}$ set the boiling heat transfer correlation (eq.23) with $x_{ev} = 0$. This is a limit condition where the liquid slug is assumend under incipient boilig

so it is still completely liquid but heat input rate plays an important role on the heat transfer coefficient.

- if $T_w < T_{fluid}$ set single phase liquid HTC (eq.19,20,21).

For the Vapor Plugs:

- if $T_w > T_{fluid}$ set boiling HTC (eq.23) with x_{ev} chosen with the hel of equation 22.
- if $T_w < T_{fluid}$ set condensation HTC (eq.24) with x_{co} chosen with the hel of equation 22.

Input parameters, initial and boundary conditions

Design parameters:

The functions that rule the PHP geometry, orientation with respect to gravity and the heat input/output zones were modified in order to automatically build a "comb geometry" (fig.4) by setting only six parameters:

- L_{ev} = evaporator section length.
- L_{co} = condenser section length.
- L_{ad} = adiabatic section length.
- L_1 = characteristic distance between turn and bend.
- r_t = radius of all bends and turns (details in fig.4).
- N_t = number of turns (180°).

The other design parameters are: the tube inner/outer diameter; the tube material (density, specific heat, thermal conductivity); the surface roughness feature size; the tilting angle; the working fluid and the filling ratio.

Computational parameters:

Maximum time step, minimum time step, refinement factor, convergence criterion, maximum allowable plug temperature change between time steps, and simulation time. The number of grid nodes comprising wall n_w, liquid n_s and turns n_k.

Boundary conditions:

Cooling medium temperature, condenser heat transfer coefficient, initial temperature, total heat input rate evaporator.

Initial conditions:

Fluid and wall temperature, initial number and distribution of the liquid and the vapor plugs. In the present work all the simulations start with an alternation of three liquid slugs and three which are equally distributed inside the PHP. Further work is mandatory to define this initial condition with a statistical approach.

NUMERICAL INVESTIGATIONS

The simulation input parameters for the present numerical campaign are listed in tables 3 and 4. The first column shows the inputs related to an arbitrary set of test cases and the second shows the inputs extrapolated from a real experimental test-rig which has been built by Yang et al. (2008). The numerical investigation focuses on the effect of four main parameters:

- The number of turns N_t (two cases with 3 and 9 turns as depicted in fig.4 plus the 39 turns);
- The input heat flux *q'' [W/cm^2]* that can be calculated from the total heat input rate and the evaporator geometry (according to figure 4) as follows:

$$q'' = \frac{\dot{Q}_{ev}}{A_{rad,ev}} \quad \text{where} \quad A_{rad,ev} = (\pi r_t + 2L_2) * \pi d_i \qquad (25)$$

- The inclination angle with respect to horizontal θ *[deg]*. As resumed in table 4, three positions were considered: 0° when the PHP lies in the horizontal position (H); 90° when the PHP is in vertical position and the evaporator is on the bottom (Bottom Heat Mode BHM); 45° is the intermediate inclination respectively between BHM and H.
- The gravity field level: Terrestrial, martian, lunar and microgravity (near to zero-g).

Notice that the momentum equation term due gravity depends on the inclination angle θ so when the PHP is in the horizontal position the gravity term is absent. In this work the results obtained for the horizontal position in normal gravity conditions are used also to describe the PHP behavior in microgravity conditions in every position. It is very important to remark that the PHP behavior in microgravity conditions has been poorly documented and that the model still needs an experimental validation on this side.

RESULTS

The choice of the code output parameters is based on the possibility of comparison with experimental measurements. Since one of the main target of the CLPHP is to keep a threshold temperature in the evaporator zone (i.e. electronic components are in contact with the PHP evaporator), the maximum tube wall temperature is one of the most critical parameters and must be monitored (fig.5-b,6-b). The total liquid momentum gives important information about the fluid flow inside the device: oscillation, circulation, reversals and eventual stops (fig.5-a,6-a).

It is evident that when the input heat flux raises from 8 to 12 *[W/cm^2]* the fluid flow inside the CLPHP with three turns changes radically. Figure 5-a shows that the total liquid momentum of the liquid phase keeps on switching between positive and negative values always maintaining an oscillating component. This means that the fluid is subjected to continuous flow reversals. These frequent changes in the flow direction are reflected also in the maximum tube temperature trend (fig 5-b). Even if the system reaches a sort of pseudo steady state after about 50 seconds, temperature is still strongly oscillating around a mean value of about 64°C with local maximum peaks at 71-72°C corresponding to the flow reversals and periods of relatively stable temperature when the circulatory motion component is more stable. On the contrary when *q"= 12[W/cm^2]* the vapor expansion in the evaporator zone is strong enough to avoid flow reversal and also the maximum tube temperature trend is more stable.

Khandekar and Groll (2004) proved the existence of frequent flow reversal on the single closed loop PHP which is even more sensible to these phenomena. Flow reversals are more frequent when the number of turns is small and for low heat flux inputs. This combination has a negative influence on the PHP performance and can be avoided by increasing the number of turns.

Effect of the number of turns in combination with the inclination angle.

Charoensawan and Terdtoon (2008) demonstrated that that CLPHP cannot work in the horizontal position if the number of turns is below a critical number. In particular all the experimented test cases with $N_t \leq 5$ did not show any fluid motion inside the tube.

Usually, when the PHP operation is stable, the number of vapor plugs is quite variable and, on average, higher than the number of heating and cooling sections. In the simulated test case with $N_t = 3$ in the horizontal position, the number of vapor plugs reduces to the number of heating sections, the fluid motion is damped and completely stops after 100 seconds as shown in figure 7-a. The device works only by conduction within the copper tube and the maximum tube temperature consequently rises towards very high values (fig 7-b). This result is qualitatively closer to the actual behaviour of a real PHP where this condition usually leads to the dry-out of the system.

On the other hand the CLPHP with nine turns is able to work as shown in figures 8-a and 8-b. Of course the oscillations amplitude is lower if compared to the gravity assisted vertical position (also called Bottom Heat Mode).

If the number of turns increases, the fluid undergoes more local instabilities, this may help to avoid the recoiling of all the liquid phase within the condenser zone and all the vapour phase in the evaporator zone and the consequent flow stop. Numerical models, that do not account for local pressure losses due to bends, cannot adequately evaluate the effect of the number of turns, in particular in the horizontal operation.

Effect of the input heat flux in combination with the inclination angle.

The thermal performance of the CLPHP has been estimated in terms of mean equivalent thermal resistance as follows:

$$R_{eq} = \left(\overline{T}_{w,\max} - \overline{T}_{\infty}\right) / \dot{Q}_{ev} \qquad (26)$$

Where $\overline{T}_{w,\max}$ and $\overline{T}_{w,\min}$ are respectively the time-average value of the maximum and minimum wall temperature when the pseudo steady state is reached.

Figure 9 shows the values of $\overline{T}_{w,\max}$ and the standard deviation bar relative to the temperature oscillation for each test case. The tilted and horizontal PHP with 9 turns are working but, since the total liquid momentum is less and less assisted by gravity forces the fluid motion becomes less vigorous and oscillation amplitude has lower values. Consequently the convective heat transfer coefficient of the liquid phase is lower and this results in higher mean maximum tube temperatures as expected from experimental evidence.

In all cases the equivalent thermal resistance (fig.10) decreases with the heat flux .

The PHP which is working in the horizontal mode reaches a minimum in the thermal resistance and a further heat input increase worsen the PHP performance. Experimental evidence suggests that beyond this heat input level dry-out will occur. Both mean maximum tube temperature and equivalent thermal resistance trends reflects (qualitatively) the experimental results obtained by Yang et al. (2008).

A Fast Fourier Transform (sample rate 20Hz) has been performed on the total liquid momentum output in order to investigate if the fluid oscillates with a characteristic frequency.

Figure 11 shows that the dominant frequencies of flow oscillations are in the range of 0.3 to 2.5Hz. These values are also confirmed by experimental data from Kim et al. (2003) and from the recent work by Khandekar et al. (2009). Looking at the present numerical results it also seems that higher oscillation frequencies bring to a better PHP thermal performance but this issue has to be further investigated also from the experimental point of view.

Effect of the input heat flux in combination with the gravity level.

In this section the PHP is set in the Bottom Heat Mode and tested for different gravity levels and different heat input rates. As expected, the trends obtained by decreasing the gravity level (figures 12, 13 and 14), are comparable to the tilted PHP trends.

If the experimental results will confirm that the horizontal operation under normal gravity is also representative of the zero gravity condition, the CLPHP could be considered a suitable candidate not only for ground but also for aerospace applications. The PHP performance in 0-g will be lower than the gravity assisted mode (Bottom Heat Mode) but it will be also independent from the inclination angle.

From the numerical investigation it seems that by decreasing the gravity level the maximum efficiency occurs at lower heat input fluxes. Figure 13 shows that the PHP with nine turns reaches the minimum equivalent thermal resistance at around $q''= 12[W/cm^2]$ at 0-g which is still comparable to the grooved and screen mesh heat pipes heat fluxes capabilities.

Oscillation frequencies are also in the range but it is hard to find a general trend related to gravity. In general higher frequencies results for higher heat inputs.

QUANTITATIVE VALIDATION

This paragraph is devoted to the validation of the present numerical model based on a recent experiment by Yang et al. (2008). Their PHP device is surely closer to an industrial application since the number of turns is high ($N_t = 39$), there is no adiabatic zone and the condenser zone, which occupies more of the 95% of the tube length, is cooled by mean of air at a constant temperature (see table 3).

Geometry, boundary and initial conditions have been extrapolated (table 3) and set as input parameters in the code; the maximum tube temperature and the equivalent thermal resistance of the system (fig.15) have been estimated for PHP operating at normal gravity, in Bottom Heat Mode for four different heat input rates.

Table 5 resumes the validation showing the maximum tube temperature in the evaporator zone and the relative error between experimental and numerical results on the equivalent thermal resistance of the system.

CONCLUSIONS

A comprehensive numerical model of CLPHP has been proposed and its response has been tested by varying three fundamental parameters: number of turns, input heat flux and inclination angle. It can be concluded that:

- Numerical models cannot adequately evaluate the effect of the number of turns if they do not account for local pressure losses due to bends, in particular in the horizontal operation.
- Numerical results confirm that for small number of turns and small input heat fluxes the CLPHP in Bottom Heat Mode may undergo flow reversals which have negative influence on the performance.
- The simulated CLPHP with three turns can only operate if gravity assisted (Bottom Heat Mode) while the CLPHP with nine turns works also in the Horizontal position even if with a lower thermal performance.
- Dominant frequencies of flow oscillations are in the range of 0.3 to 2.5Hz (quantitatively confirmed by experimental data). If the PHP is operating in the “pure oscillation mode” higher oscillation frequencies are connected to a better PHP thermal performance. However, CLPHPs operate best in the "circulation

mode" where oscillation frequencies are of no importance. This is also demonstrated in figs.5-a,b vs. figs.6-a,b.

- Numerical results (mean maximum tube temperature, equivalent thermal resistance trends) reflects the qualitative experimental trends. Good quantitative matching have been also found for a real test case with 39 turns, operating with R123 as working fluid in the Bottom Heat Mode.
- If future experimental results will confirm that the horizontal operation under normal gravity is also representative of the zero gravity condition, the CLPHP could represent a suitable candidate not only for ground but also for space applications.

REFERENCES

Akachi, H.: Structure of a heat pipe, U.S. patent 4,921,041 (1990).

Akachi, H.: Structure of a micro heat pipe, US patent 5,490,558, (1993).

Carey, Van P.: Liquid-vapor phase-change phenomena. Taylor&Francis, (2007).

Charoensawan, P. ,Terdtoon, P.: Thermal performance of horizontal closed-loop pulsating heat pipes. App. Therm. Eng., 28, 460-466, (2008).

Darby R.: Correlate pressure drop through fittings. Chem. Eng., 101–104, (1999).

Darby R.: Correlate pressure drop through fittings. Chem. Eng., 127–130, (2001).

Gu, J., Kawaji, M., Futamata, R.: Effects of gravity on the performance of pulsating heat pipes. J. of Thermophisycs and Heat Transfer, 18(3), 370-378, (2004).

Gu, J., Kawaji, M., Futamata, R.: Microgravity performance of micro pulsating heat pipe. Microgravity Sc. and T. , 16, 181-185, (2005).

Han Y., Shikazono N.: Measurement of the liquid film thickness in micro tube slug flow. Int. J. of Heat and Fluid Flow, 30, 842–853, (2009).

Holley, B., Faghri, A.: Analysis of pulsating heat pipe with capillary wick and varying channel diameter. Int. J. of Heat and Mass Transfer, 48, 2635–2651, (2005).

Incropera, F.P., DeWitt, D.P.: Fundamentals of heat and mass transfer. Sixth edition, Wiley, (2007).

Khandekar S., Groll, M.: Roadmap to realistic modeling of closed loop pulsating heat pipes. Proc. of the 9th International Heat Pipe Symposium, Kuala Lumpur, Malaysia, November (2008).

Khandekar, S., Gautam, A.P., Sharma, P.K.: Multiple quasi-steady states in a closed loop pulsating heat pipe. Int. J. of Thermal Sciences, 48, 536-546, (2009).

Khandekar, S., Groll, M.: An insight into thermo-hydrodynamic coupling in closed loop pulsating heat pipes. Int. J. of Thermal Sciences, 43, 13-20, (2004).

Khandekar, S.: Pulsating heat pipe based heat exchangers. Proc. Of the 21st Int. Symposium on Transport Phenomena, Kaohsiung City, Taiwan, 2-5 November, (2010).

Kim J.S., Bui N.H., Jung H.S., Lee W.H.: The study on pressure oscillation and heat transfer characteristics of oscillating capillary tube heat pipe. KSME International Journal, 17(10), 1533-1542, (2003).

Mameli, M. , Marengo, M. ,Zinna, S.: Thermal simulation of a pulsating heat pipe: effects of different liquid properties on a simple geometry. Proc. of the 7th Int. Conf. on Heat Transfer, Fluid Mechanics and Thermodynamics, 19-21 July, Antalya, Turkey, (2010).

Miyazaki, Y.: Cooling of notebook pcs by flexible oscillating heat pipes. Proc. of ASME INTERPACK, San Francisco, California, USA, July 17-22, (2005).

Rittidech, S., Wannapakne S.: Experimental study of the performance of a solar collector by closed-end oscillating heat pipe. App. T. Eng., 27, 1978–1985, (2007).

Sakulchangsatjatai P., Chareonsawan, P., Waowaew, T., Terdtoon, P., Murakami, M.: Mathematical modelling of closed-end pulsating heat pipes operating with a bottom heat mode. Heat Transfer Eng., 29(3), 239-254, (2008).

Shafii, M.B., Faghri, A., Zhang, Y.: Thermal modeling of unlooped and looped pulsating heat pipes. ASME Journal of Heat Transfer, 123, 1159-1162, (2001).

Shah, R.K.: Thermal entry length solutions for the circular tube and parallel plates. Proc. 3rd National Heat Mass Transfer Conference, IIT Bombay, Vol. I, Paper HMT-11-75, (1975).

Woo, J., Kim, J., Han, K., Ahn, S.: A study on cooling performance of heat sink using pulsating heat pipe. Proc. of the 9th Int. Heat Pipe Symposium, Kuala Lumpur, Malaysia, November 17-20, (2008).

Yang, H. ,Khandekar, S. ,Groll, M.: Operational limit of closed loop pulsating heat pipe. App. Therm. Eng., 28, 49-59, (2008).

Zhang, Y., Faghri, A.: Oscillatory flow in pulsating heat pipes with arbitrary numbers of turns. J. of Thermophysics and Heat Transfer, 17(3), 340-347, (2003).

Zuo, Z. J., North M. T., Ray, L.: high heat flux heat pipe mechanism for cooling of electronics. IEEE transactions on components and packaging technologies. 24, 2, 220-225, (2001).

Zuo, Z. J., North, M. T., Ray L.: Combined pulsating and capillary heat pipe mechanism for cooling of high heat flux electronic. Internal Report, Thermacore Inc., (2001).

List of figures:

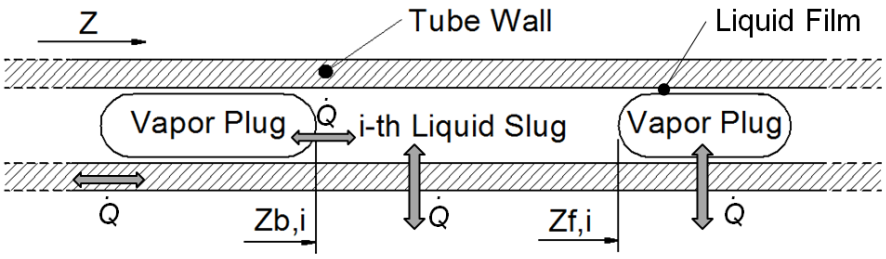

Figure 1: Schematic the flow pattern and heat transfer process in the PHP model.

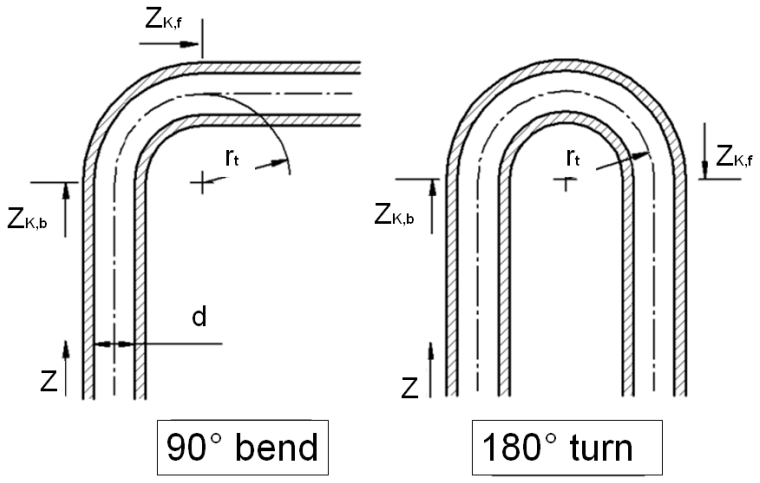

Figure 2: Geometry of 90° bend and 180° turn in the CLPHP.

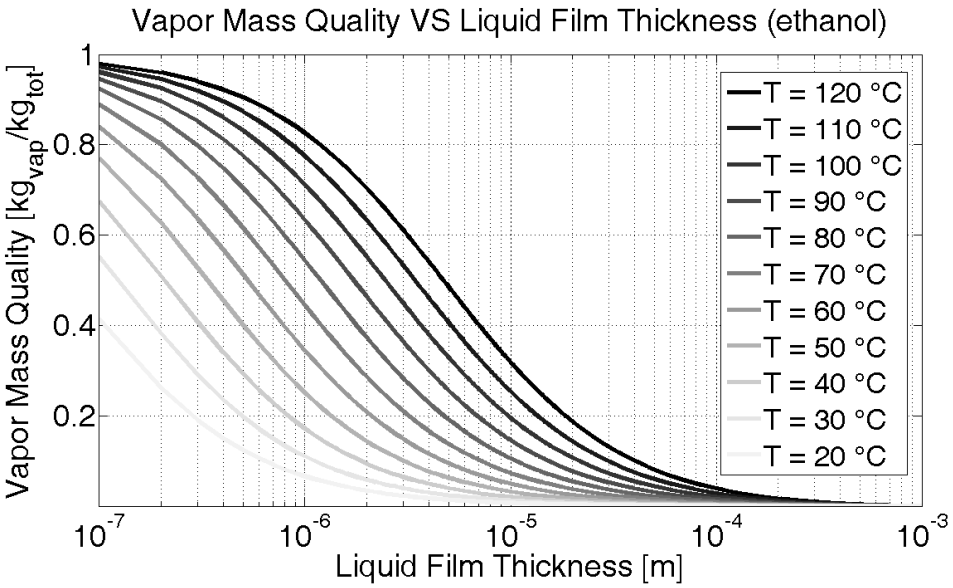

Figure 3: Ethanol quality over liquid film thickness for different fluid temperatures.

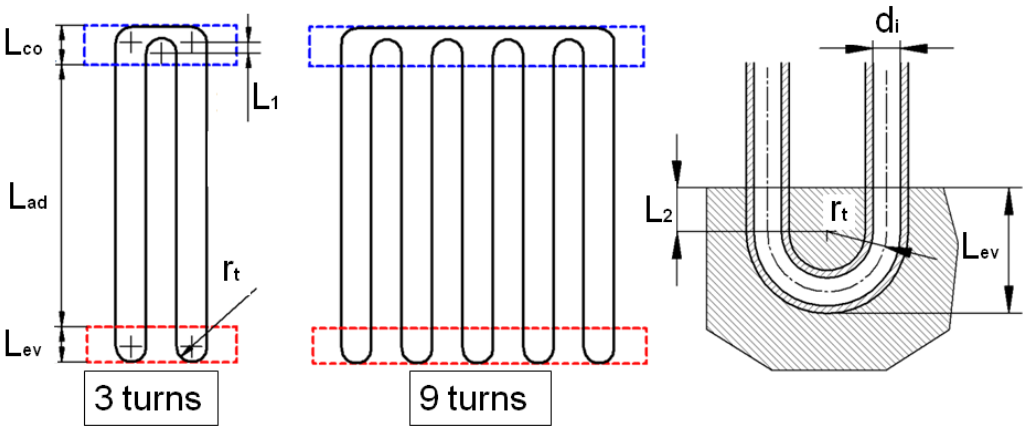

Figure 4: CLPHP geometry input parameters..

.

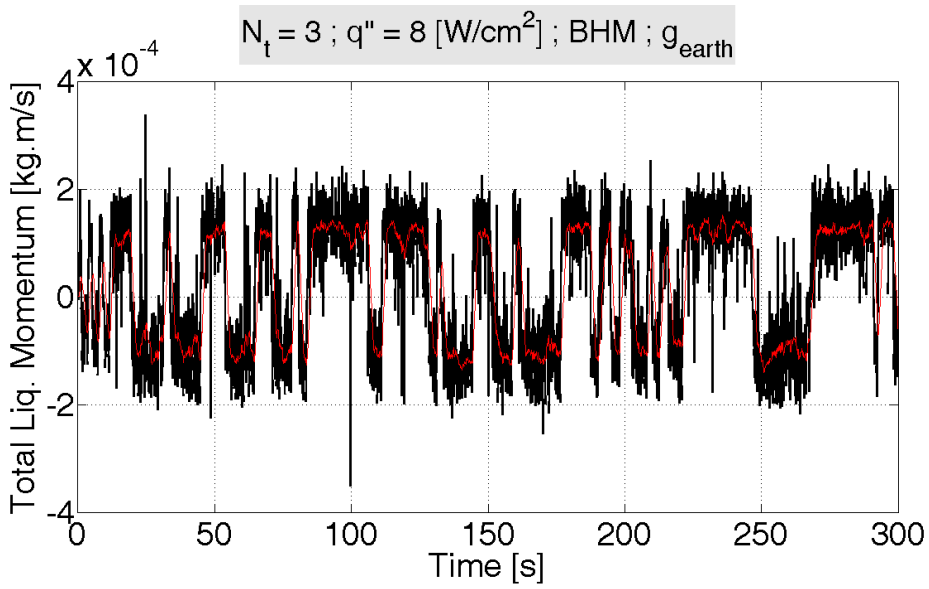

Figure 5-a: Total Liquid Momentum VS time for the 3 turns CLPHP with *q"= 8[W/cm²]* in Bottom Heat Mode and normal gravity conditions.

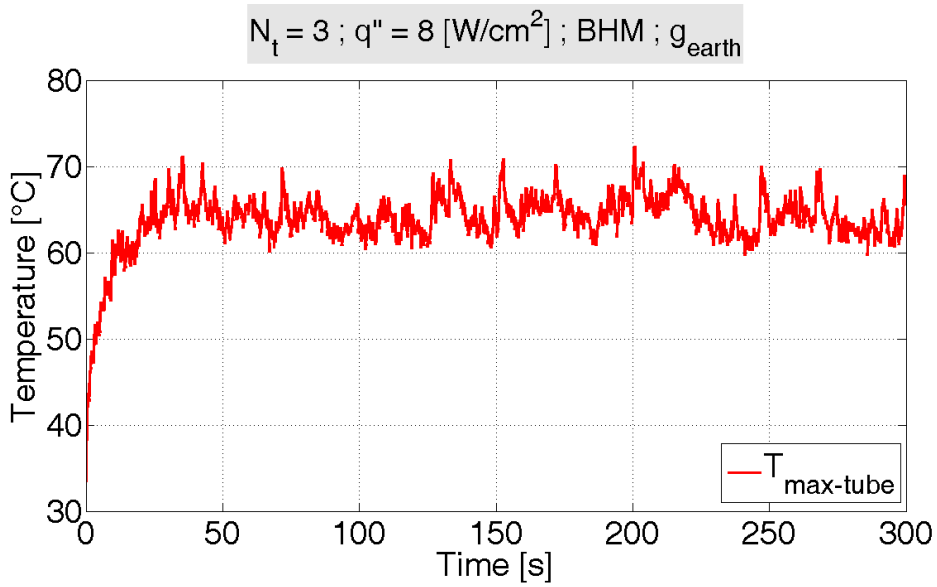

Figure 5-b:Maximum Tube Temperature VS time for the 3 turns CLPHP with *q"= 8[W/cm²]* in Bottom Heat Mode and normal gravity conditions.

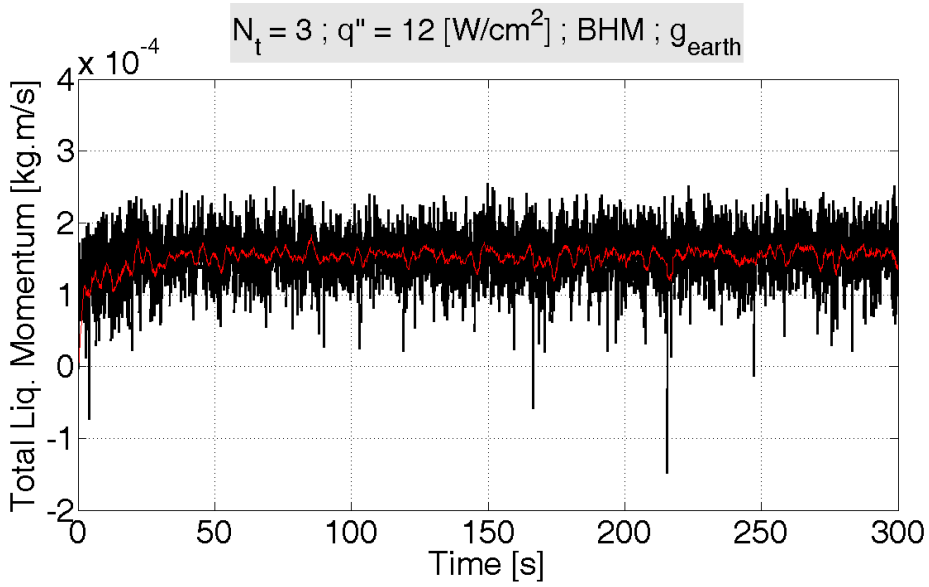

Figure 6-a: Total Liquid Momentum VS time for the 3 turns CLPHP with *q"= 12[W/cm²]* in Bottom Heat Mode and normal gravity conditions.

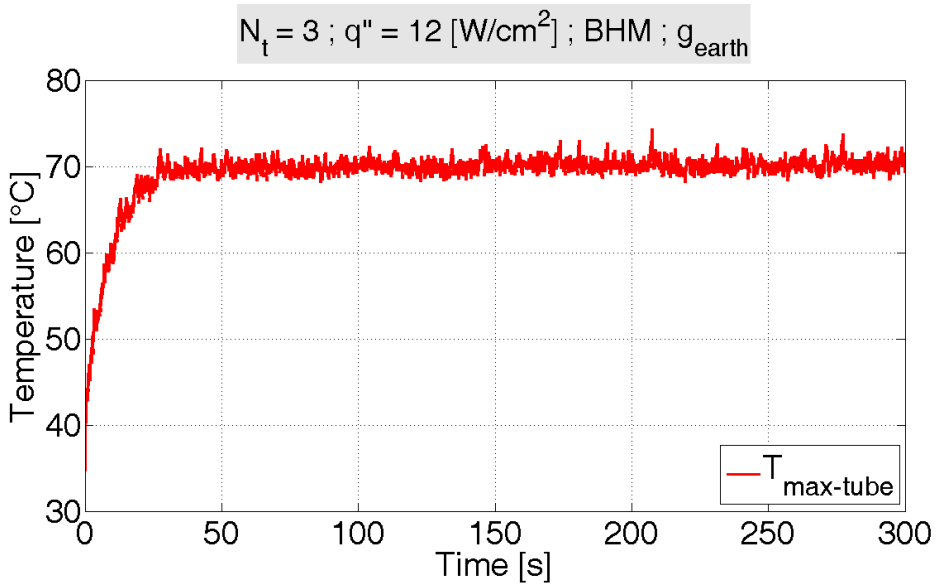

Figure 6-b: Maximum Tube Temperature VS time for the 3 turns CLPHP with *q"= 12[W/cm²]* in Bottom Heat Mode and normal gravity conditions.

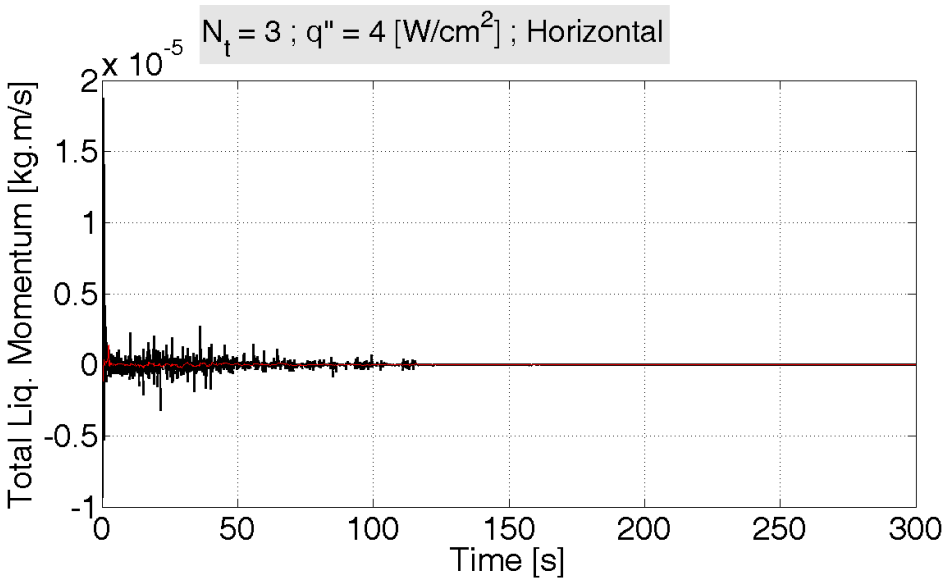

Figure 7-a: Total Liquid Momentum VS time for the 3 turns CLPHP with *q"= 4[W/cm²]* in Horizontal Mode.

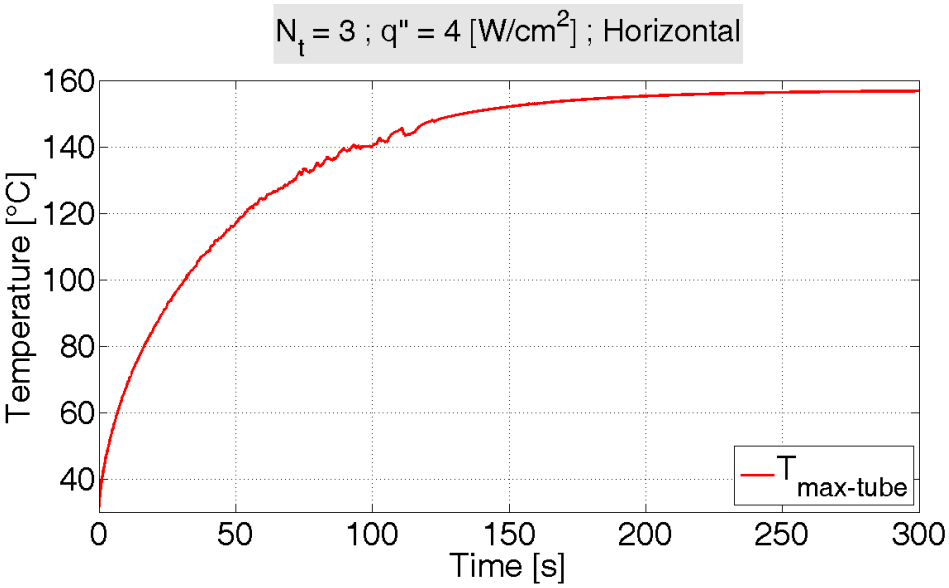

Figure 7-b: Maximum Tube Temperature VS time for the 3 turns CLPHP with *q"= 4[W/cm²]* in Horizontal Mode.

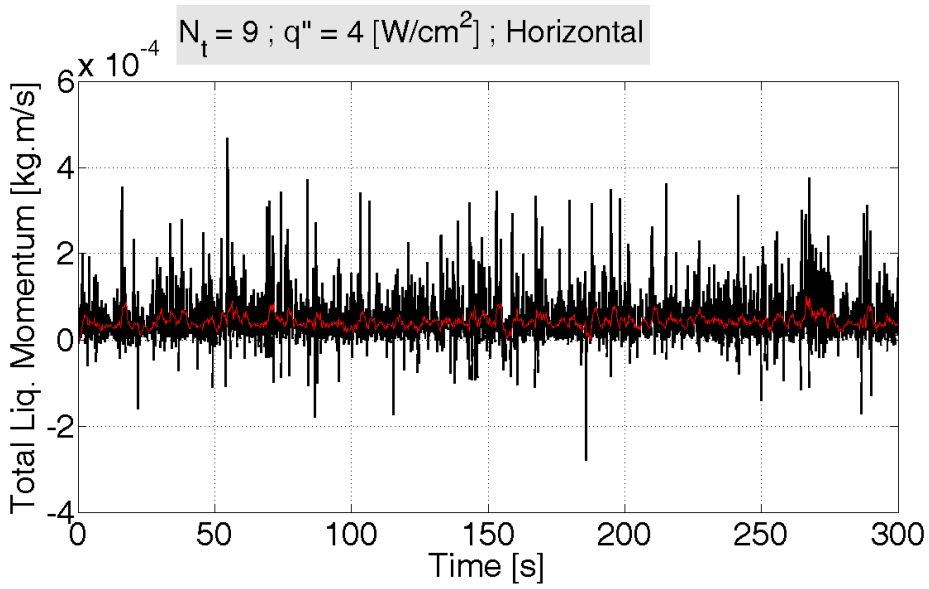

Figure 8-a: Total Liquid Momentum VS time for the 9 turns CLPHP with *q"= 4[W/cm²]* in Horizontal Mode.

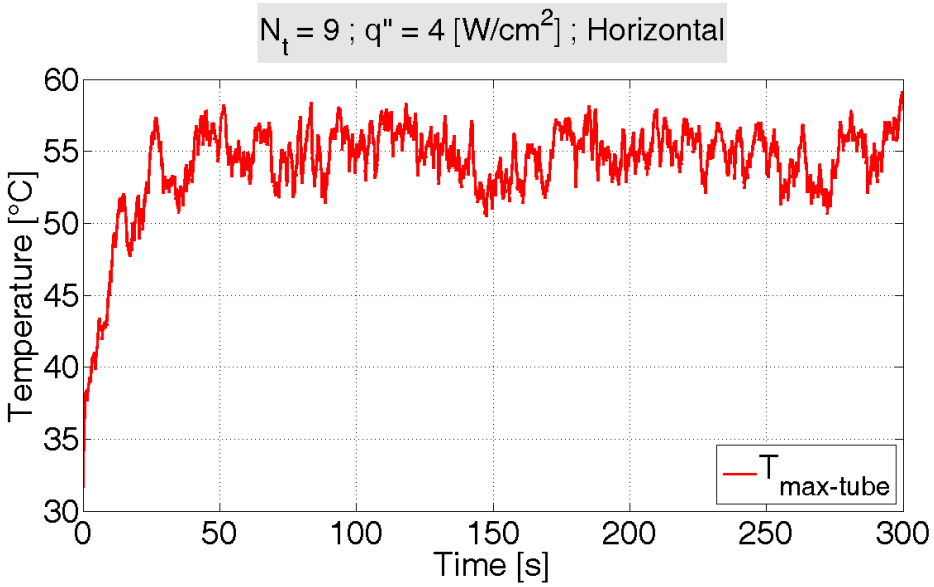

Figure 8-b: Maximum Tube Temperature VS time for the 9 turns CLPHP with *q"= 4[W/cm²]* in Horizontal Mode.

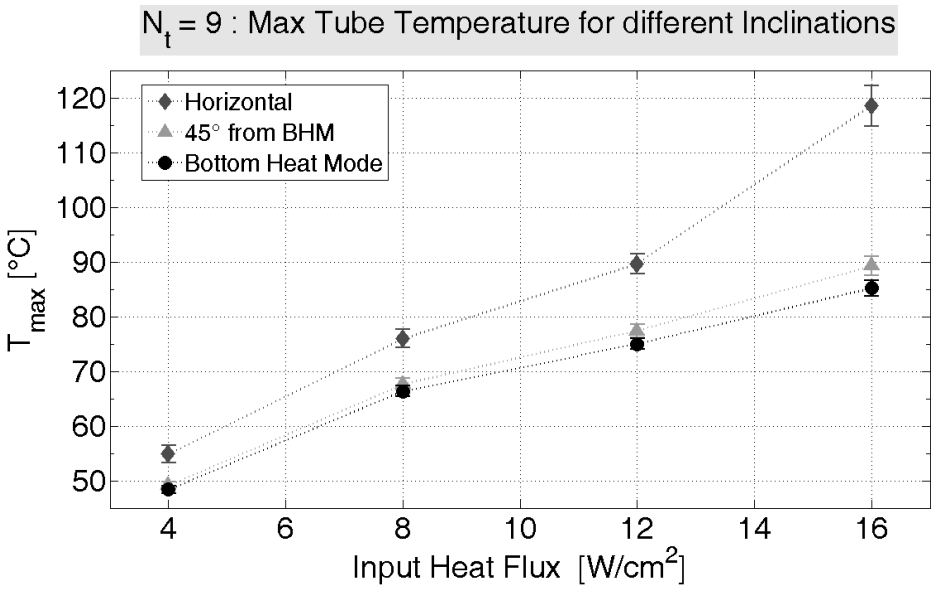

Figure 9: Mean Maximum Tube Temperature VS Input Heat Flux for the 9 turns CLPHP at different orientations.

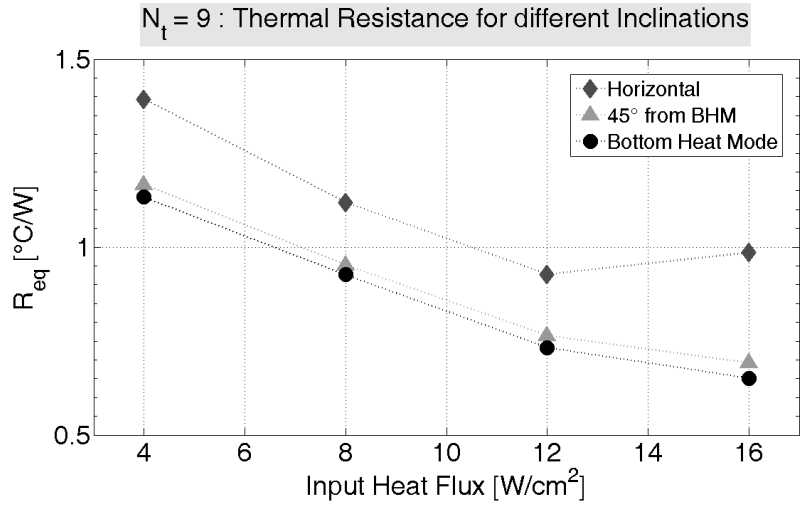

Figure 10: Equivalent Thermal Resistance VS Input Heat Flux for the 9 turns CLPHP at different orientations.

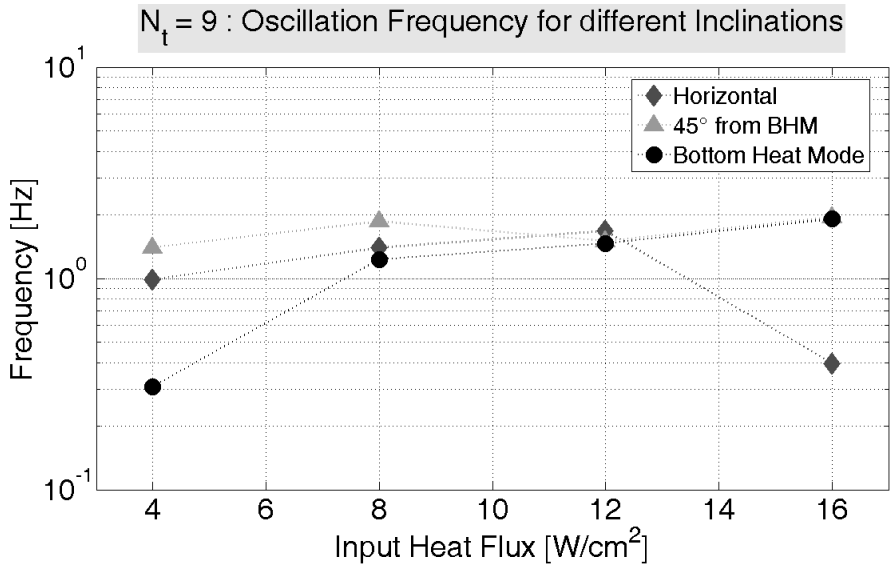

Figure 11: Characteristic frequency of the Total Liquid Momentum oscillation VS Input Heat Flux for the 9 turns CLPHP at different orientations.

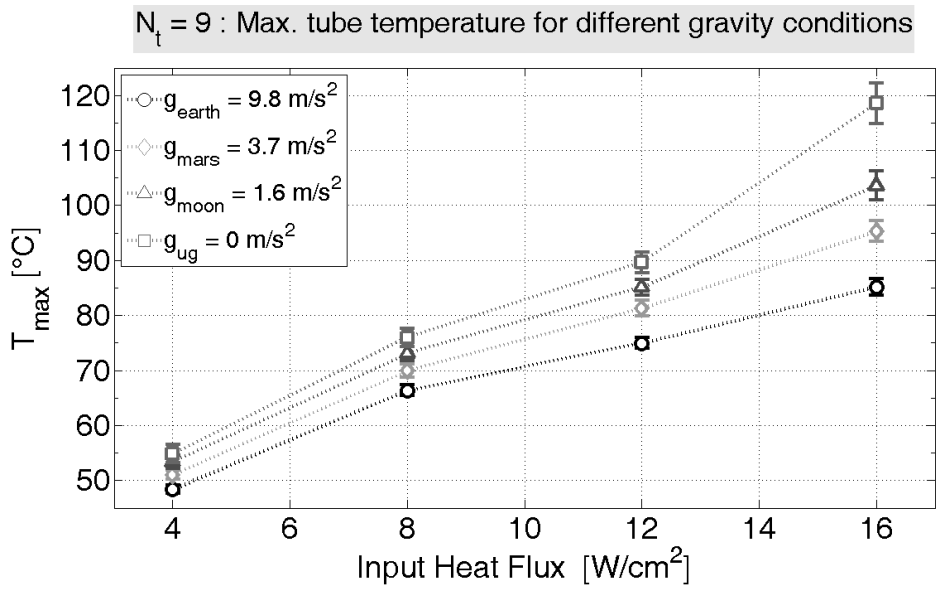

Figure 12: Mean Maximum Tube Temperature VS Input Heat Flux for the 9 turns CLPHP at gravity levels.

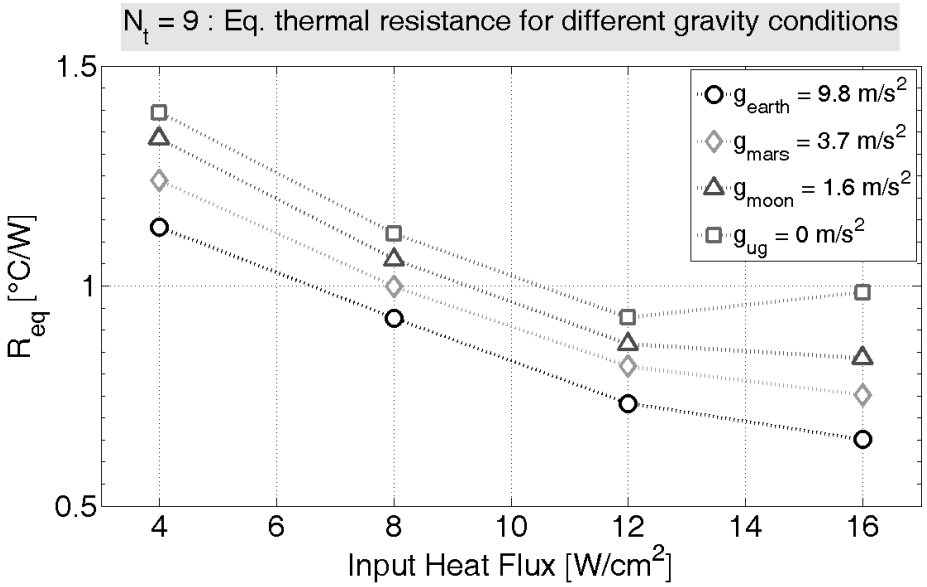

Figure 13: Equivalent Thermal Resistance VS Input Heat Flux for the 9 turns CLPHP at different gravity levels.

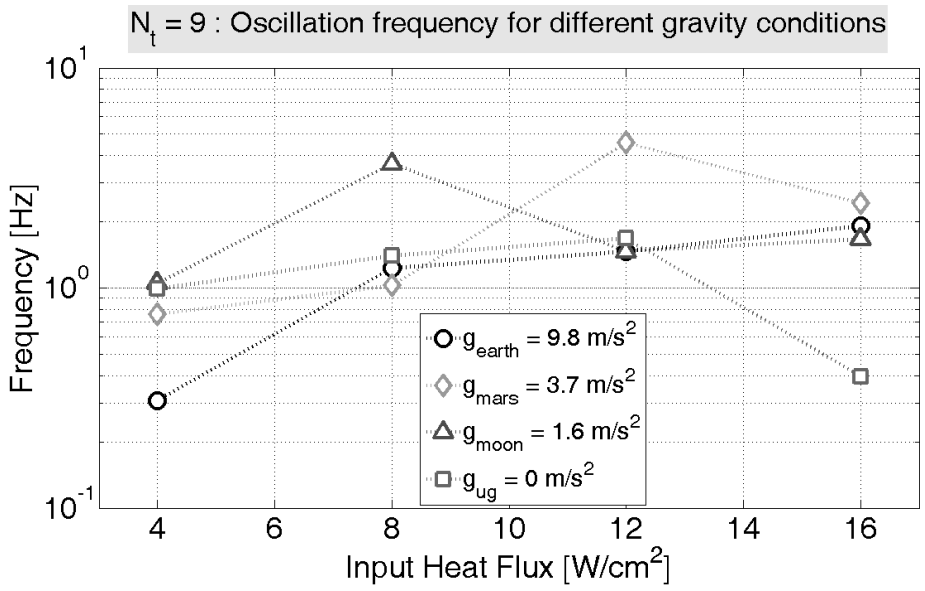

Figure 14: Characteristic frequency of the Total Liquid Momentum oscillation VS Input Heat Flux for the 9 turns CLPHP at different gravity levels.

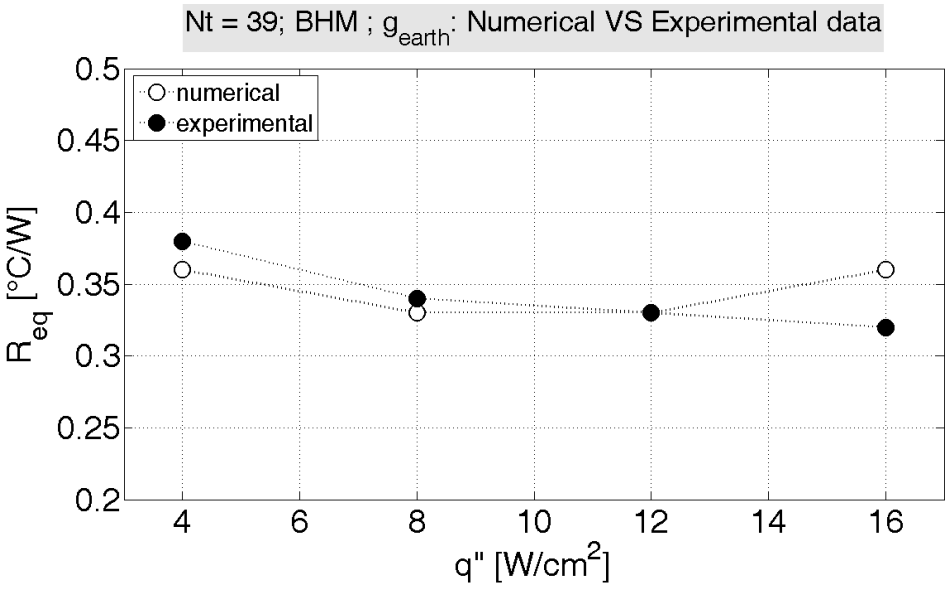

Figure 15: Comparison between numerical results and the experimental data obtained by Yang et al. (2008) on the 39 turns CLPHP operating in Bottom Heat Mode.

List of tables

Table 1: 3-K constants for loss coefficients for bends and turns according to Darby.

Fitting type	r_t/d	K_{Re}	K_r	K_d
bend 90°	1.25	800	0.091	4
Turn 180°	1.25	1000	0.1	4
bend 90°	2.5	800	0.056	3.9
Turn 180°	2.5	1000	0.1	4

Table 2: Choice of the vapor mass quality for evaporating and condensing vapour plugs (values obtained for ethanol).

q'' [W/cm^2]																
4				8				12				16				
$T_{fluid,min}$ [°C]		$T_{fluid,max}$ [°C]		$T_{fluid,min}$ [°C]		$T_{fluid,max}$ [°C]		$T_{fluid,min}$ [°C]		$T_{fluid,max}$ [°C]		$T_{fluid,min}$ [°C]		$T_{fluid,max}$ [°C]	
23		55		34		70		54		87		76		117		
$x_{vp,min}$	$x_{vp,max}$	$x_{vp,min}$	$x_{vp,max}$	$x_{vp,min}$	$x_{vp,max}$	$x_{vp,min}$	$x_{vp,max}$	$x_{vp,min}$	$x_{vp,max}$	$x_{vp,min}$	$x_{vp,max}$	$x_{vp,min}$	$x_{vp,max}$	$x_{vp,min}$	$x_{vp,max}$
0.0007	0.0772	0.0036	0.2960	0.0013	0.1320	0.0065	0.4343	0.0034	0.2867	0.0130	0.6074	0.0083	0.4944	0.0355	0.8116
$x_{vp,co}$		$x_{vp,ev}$		$x_{vp,co}$		$x_{vp,ev}$		$x_{vp,co}$		$x_{vp,ev}$		$x_{vp,co}$		$x_{vp,ev}$	
0.001		**0.01**		**0.01**		**0.1**		**0.1**		**0.5**		**0.4**		**0.8**	

Table 3: Main set of input parameters.

INPUT PARAMETER	**CLPHP with 3 and 9 turns**	**CLPHP with 39 turns**
Working Fluid	ethanol	R123
Tube thermal conductivity	$K_w = 400$ W/mK	$K_w = 400$ W/mK
Tube specific heat capacity	$c_{p,w} = 389$ J/kgK	$c_{p,w} = 389$ J/kgK
Tube density	$\rho_w = 8960$ kg/m^3	$\rho_w = 8960$ kg/m^3
Internal tube diameter	$d_{in} = 2$mm	$d_{in} = 2$mm
external tube diameter	$d_{out} = 3$mm	$d_{out} = 3$mm
Inner surface roughness	$r_{fs} = 50$ µm	$r_{fs} = 50$ µm
Curvature radius of all bends and turns	$r_t = 2.5$mm	$r_t = 5$mm
Adiabatic section length	$L_{ad} = 102$mm	$L_{ad} = 0$mm
Evaporator section length	$L_{ev} = 8.5$mm	$L_{ev} = 7$mm
Condenser section length	$L_{co} = 8.5$mm	$L_{co} = 8.5$mm
Total length	$L_{tot} = 440$mm $L_{tot} = 1100$mm	$L_{tot} = 5040$mm
fluid initial temperature	$T_0 = 30$ °C	$T_0 = 30$ °C
filling ratio	$\gamma = 0.6$	$\gamma = 0.5$
condenser ext. heat transfer coefficient	*(constant temperature boundary condition)*	$h_\infty = 90$ W/m^{2}K
external cooling temperature	$T_\infty = 20$ °C	$T_\infty = 27$ °C

Table 4: resume of the numerical simulation campaign.

	CLPHP 1	**CLPHP 2**	**CLPHP 3**
N_t	**3**	**9**	**39**
$A_{rad,ev}$[cm^2]	2.49	6.23	25.13

$\dot{Q}_{ev}[W]$	10; 20; 30; 40	25; 50; 75; 100	100; 200; 300; 400
θ [deg]	**three positions: 0°; 45; 90°**		**Bottom Heat Mode (90°)**
g [m/s²]	**Four gravity levels: 9.81 (earth); 3.69 (mars); 1.6 (moon); ≈ 0 (microgravity)**		**9.81 (earth)**
q" [W/cm²]	**Four cases: 4; 8; 12; 16**		

Table 5: Numerical results VS Experimental data.

q" [W/cm²]	***Q [W]***	***Te_{exp} [°C]***	***Te_{num} [°C]***	***R_{eq-exp} [°C/W]***	***R_{eq-num} [°C/W]***	***Err. on R_{eq} [%]***
4	100	65	63	0.38	0.36	5.26
8	200	95	93	0.34	0.33	2.94
12	300	126	127	0.33	0.33	1.01
16	400	155	170	0.32	0.36	11.72